European Journal of Mechanics B/Fluids 29 (2010) 259–268

Contents lists available at ScienceDirect

European Journal of Mechanics B/Fluids

journal homepage: www.elsevier.com/locate/ejmflu

On the flow field generated by a gradually varying flow through an orifice

Giorgio Querzoli [a], Massimo Falchi [b], Giovanni P. Romano [c,*]

[a] Dipartimento di Ingegneria del Territorio, Università di Cagliari, Cagliari, Italy
[b] INSEAN, The Italian Ship Model Basin, Roma, Italy
[c] Dipartimento di Meccanica e Aeronautica, Università "La Sapienza", 184 Roma, Italy

ARTICLE INFO

Article history:
Received 12 January 2009
Received in revised form
7 January 2010
Accepted 11 March 2010
Available online 21 March 2010

Keywords:
Vortex ring
PIV
Time scaling
Slug model

ABSTRACT

The motion of a vortex ring generated by gradually varied flows through a thin-edged orifice has been investigated experimentally using particle image velocimetry. This flow reproduces the primary characteristics of many biological flows, such as cardiac flows through valves or jellyfish and squid propulsion. Even though vortex ring formation has been extensively studied, there is still interest in gradually varying inflows, i.e. the ones that are mostly found in previous conditions. The main purpose of this paper is to extend the time scaling already proposed in the literature to the entire cycle of vortex ring formation, pinch-off and free motion. To this end, eight inflow time laws have been tested, with different acceleration and deceleration phases. They have been selected in relation to practical applications by their resemblance to the main characteristics of cardiovascular and pulsed locomotion flows. Analysis of measured velocity and vorticity fields suggested a general criterion to establish the instant of vortex pinch-off directly from the imposed velocity program. This allows the proper scaling of the entire time evolution of the vortex ring for all tested inflows. Since it is quite easy to identify this instant experimentally, these results give a simple, practical rule for the computation of scales in vortex ring formation and development in the case of gradual inflows. The "slug model" has been used to test the proposed scaling and to obtain predictions for the vortex position, circulation and vorticity which are in agreement with experimental data.

1. Introduction

The sudden onset of a jet in a fluid at rest generates a vortex ring that begins to travel in the direction of the jet axis. Typically, the vortex ring grows up to a limiting value and, if the flow continues further, it detaches from the trailing jet which no longer contributes to the increase of its circulation but rather produces a vorticity layer in its wake. Understanding this type of phenomenon is of fundamental importance for a wide range of applications, such as intraventricular flows and the propulsion of aquatic animals. The link between the characteristics of the jet flow and the features of the resulting vortex ring has been investigated extensively in the past [1,2]. Theoretical analysis and modelling, such as those of Tung and Ting [3] and Saffman [4], predicting the travel velocity of a viscous vortex ring, and the study by Pullin [5], using similarity theory to predict the main parameters of vortex rings originated both by tubes and orifices have been also carried out. On the basis of experimental observations [6], Mohseni and Gharib [7] suggested an analytical model predicting a parameter limiting their growth, i.e. a limiting value for the circulation around the vortex ring. Kaplanski and Rudi [8] proposed a model that also accounted for the viscosity, while Krueger [9] included the pressure field by showing that this correction is important only in the presence of sudden temporal variations. Experimental investigations were initially based on visualisations [10,11], revealing that the details of the forcing used to push the flow through the orifice are important. With the advent of digital imaging, many investigators began to use particle image velocimetry (PIV) to measure velocity and vorticity fields [12–15]. In particular, Gharib et al. [6] determined the time of pinch-off and introduced the idea of a limiting non-dimensional time in the development of the vortex rings. Krueger and Gharib [16] used PIV and hot film anemometry to explore the relation between the velocity field originated by a starting jet and the resulting thrust.

Though it is well known that this phenomenon is affected by the so-called velocity program, i.e. the variation of the flow rate with time, most investigators have focused their work on the development of vortex rings using very simple laws of motion: namely, constant flow rate ("impulsive program"), flow rate increasing in a linear way over time, or a combination of them in a "trapezoidal program". Glezer [10] reported results from different velocity programs and proposed a factor that should account for all the variations of the flow rate in time. In particular,

* Corresponding author.
E-mail address: romano@dma.ing.uniroma1.it (G.P. Romano).

0997-7546/$ – see front matter © 2010 Elsevier Masson SAS. All rights reserved.
doi:10.1016/j.euromechflu.2010.03.004

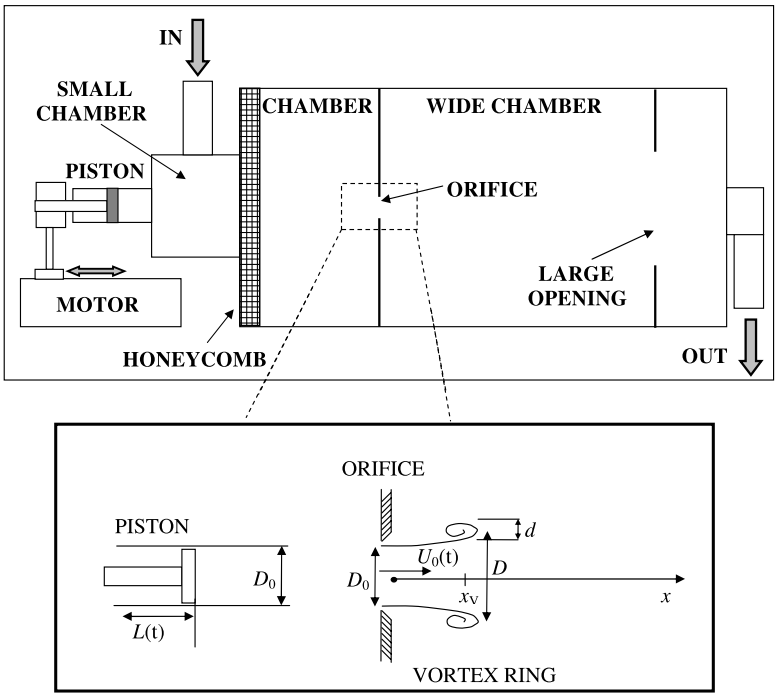

Fig. 1. Experimental set-up. Details of the orifice and piston are given in the inset.

this velocity program factor (defined as the normalised mean square value of the forcing signal) allowed for the proper scaling of vortex circulation for a wide range of velocity programs. Rosenfeld et al. [17], in a numerical simulation, noticed that pinch-off can be meaningfully delayed by using a constantly increasing flow rate. Krueger and Gharib [16] observed experimentally that negative-slope velocity programs determine earlier non-dimensional pinch-off times than positive-slope ones. Recently, Shusser et al. [18] discussed the effect of the time variation of the exit flow rate in terms of impulsive, linear and trapezoidal velocity programs.

Despite the fact that such schematic programs are conceptually easier to deal with, in nature there are cases in which the flow rate increases gradually over time and then decreases again, without any abrupt change in the slope of the curve, leading to very high (indeed, potentially infinite) peaks in acceleration [19,20]. For instance, this characteristic is typical of biological flows – such as in jellyfish [21] and squid [22] locomotion – and cardiovascular flows, such as the intraventricular flow through the mitral valve [23,24]. In such flows, the exit velocity is characterised by non-monotonic variations over time, which are expected to affect the formation of the vortex ring in a non-trivial way. In any case, there is no unequivocal event that triggers the end of that process, such as a sudden stop of the flow rate or a sharp change in the slope of the velocity program. In a recent paper, Danaila and Helie [25], following Maxworthy [26], tested the time scaling of vortex velocity and circulation at intermediate Reynolds numbers. They considered the whole process of vortex formation, pinch-off and free motion. However, it is important to note that, in this case as well, the velocity program driving the flow was impulsive with short acceleration and deceleration phases.

The purpose of this study is to reproduce the salient characteristics of biological flows in a laboratory in order to expand knowledge about vortex ring behaviours. To this end, the flow generated by gradually varying velocity programs downstream of a thin-edge orifice was investigated in the laboratory using PIV. The main question we are going to address is whether there is any simple rule which permits the reliable estimation of the scales describing all the phases of the phenomenon, including inflow acceleration and deceleration, for a large set of forcing signals. To answer this question, the velocity and vorticity fields resulting from different gradually varied velocity programs with different acceleration and deceleration behaviours have been examined. A criterion for determination of pinch-off and proper time scaling of the phenomenon is proposed by considering the instant when the inflow through the orifice does not influence the behaviour of the vortex ring anymore. The observed results are compared with predictions obtained using the so-called "slug model" [10,2]. In the next section, we will briefly describe the methods and equipment we used, whereas in Section 3 we will present the flow behaviour, model predictions, proposed scaling and experimental results. Comments and conclusions will be given at the end of the paper.

2. Materials and methods

The test section was designed to duplicate some of the remarkable characteristics of the aforementioned biological flows. In these conditions, the fluid flows from a relatively large chamber through an orifice. As a consequence, the fluid accelerates suddenly and does not develop a significant boundary layer at the walls. In addition, streamlines rapidly contract at the exit section and a *vena contracta* is found immediately after the orifice. In these ways, real biological flows differ from those generated by means of pipes or piston/cylinder arrangements widely used for the study of vortex ring development.

A sketch of the experimental set-up is shown in Fig. 1. As a result of the reciprocating motion of the piston, driven by the linear motor, the water flowed into the working tank from the inlet to the chamber (cubic, side-length: 40 cm), through a small chamber (cubic, side-length: 20 cm). The investigated flow was generated by a thin-edged orifice (the edge was made sharp all over the border as sketched in the inset of Fig. 1), with diameter $D_0 = 3.0$ cm, located at the centre of an aluminium plate, and was allowed to develop in a 60 cm long and 40 cm $\times$ 40 cm wide chamber. Finally, the fluid flowed out from a large, circular, opening (20 cm in diameter) made on a Plexiglas plate. The walls of the tank were made of 2 cm thick Plexiglas. Both the water inlet and outlet were connected to a constant-head reservoir through two one-way in and out valves.

As a consequence, the water flowed though the orifice during the forward motion of the piston and into the chamber when the piston was moving backwards. The linear motor driving the piston was controlled by a PC so that the velocity program could be arbitrarily assigned.

The vertical mid-plane of the wide chamber was illuminated with a Nd-YAG laser, producing pairs of impulses, 50 mJ each, with a 3.5 ms interframe interval. The light sheet thickness was about 2 mm. The water was seeded with calibrated hollow glass non-buoyant particles (10 μm in diameter). A cross-correlation camera, orthogonal to the light sheet, obtained pairs of $1376 \times 1040 \times 12$ bit images following a trigger signal synchronised with the motion of the motor. The resulting maximum spatial resolution was 8×10^3 m^{-1} (the entire investigated region was 12 cm large). More than 20 phases per cycle were considered (therefore, the resolution over time was about 25 s^{-1}). Considering that the frequency of oscillation of the piston was 1 Hz, these choices ensured good resolutions for the description of the whole process of vortex formation and subsequent evolution in space and time, which is the main focus of this investigation. Fifty image pairs were taken at each phase of the periodic motion of the piston; consequently, the results presented in this paper are phase averaged over 50 samples.

Velocity fields were obtained using a PIV recursive cross-correlation algorithm with window shift, deformation and Gaussian sub-pixel approximation (LaVision GmbH), using final interrogation areas of 32×32 pixels, with 75% overlap (the vector spacing equals 8 pixels, so the spatial resolution in the velocity field is 1/8th of the maximum resolution, i.e. equal to about 10^3 m^{-1}) and the set of fields measured at the same phase was averaged. The laser timing was controlled very precisely (about $\pm 1 \mu s$), so the relative error in the PIV velocity is dependent on the minimum measurable distance (± 0.1 pixel), and is around 1%.

The piston displacement was feedback controlled by computer, so that if there were a difference between the input signal and the real displacement larger than 0.2 mm the piston motion was modified accordingly. Therefore, since the average piston stroke length was 5 cm, the resulting error with regard to piston position was around 0.4%.

Eight different piston programs, all with a time period of $T = 1.0$ s, but characterised by different acceleration and deceleration phases, were tested (all ensuring continuity of functions and their derivatives within each cycle and from one cycle to the next one). The selection of these signals was performed by considering a wide class of applications to biological flows (in particular cardiovascular flows, [27–30] and small aquatic animal locomotion, [31,16]. The time laws of the displacement of the piston, $s(t)$, were

$$
\begin{aligned}
s_{1,2}(t) &= A_{1,2}\left[\frac{t}{T}\left(1-\frac{t}{T}\right)^{\frac{1-t_0}{t_0}}\right]^3,\\
s_3(t) &= A_3\left[\left(\frac{t}{T}\right)^{\frac{t_0}{1-t_0}}\left(1-\frac{t}{T}\right)\right]^3,\\
s_{4,5}(t) &= A_{4,5}\left[\alpha\left(\frac{t}{T}\right)^5+\beta\left(\frac{t}{T}\right)^4+\gamma\left(\frac{t}{T}\right)^3\right.\\
&\quad \left.+\ \delta\left(\frac{t}{T}\right)^2+\varepsilon\left(\frac{t}{T}\right)\right],\\
s_{6,7,8}(t) &= \frac{A_{6,7,8}}{2}\left(1-\cos\frac{2\pi t}{T}\right),
\end{aligned}
\tag{1}
$$

i.e. power laws (s_1, s_2, s_3), polynomial splines (s_4, s_5) and sinusoidal functions (s_6, s_7, s_8), where the amplitudes $A_{1,2,\ldots,8}$ were related to the stroke volumes ejected through the orifice. Usually a physiological value equal to 70 ml was used except for sinusoidal signals s_6 and s_8, for which 50 ml and 90 ml were selected; see Table 1. The quantity t_0 represents, in terms of the entire period T, the time at which the maximum upward displacement is attained for these signals, i.e. the time when the piston stops and starts to move backward; t_0 is equal to 0.3, 0.5, and 0.7 for programs s_1, s_2, and s_3, respectively. The coefficients $\alpha, \beta, \ldots, \varepsilon$ were computed by requiring zero values of the functions' first two derivatives at the origin, and at one intermediate point which for s_4 and s_5 were respectively $t/T = 0.3$ and $t/T = 0.5$ when an equivalent (same order with different coefficients) polynomial spline started the descending part. The coefficients $\alpha, \beta, \ldots, \varepsilon$ were also related to inverse power exponents – up to fifth order – of the time at which the maximum upward displacement was attained with programs s_4 and s_5. Each input signal was given in the form of 200 data points. The eight tested displacement and velocity programs are shown in Fig. 2a, b. It should be noted that programs s_1 and s_4 were selected because they have the typical features of the flow rate through the cardiac valves (rapid acceleration and subsequent slower deceleration). Programs s_2, s_3 and s_5 mimic the effects of time delaying the maximum value, and this is relevant in aquatic locomotion applications. Velocity programs s_6, s_7 and s_8 are sinusoidal functions with different amplitudes which were selected to investigate the effect of different stroke volumes on the evolution of the generated vortex ring. Thus, the different velocity programs cover a rather wide variety of continuously varying forcing.

Preliminary investigations ensured that before starting the piston motion the velocity and vorticity levels upstream the orifice were almost zero. The mean velocity measured at the orifice as resulting from the eight programs is also plotted in Fig. 2c as a function of time. The time interval between the investigated phases was 50 ms. Comparing these curves with those imposed at the piston, it can be noted that the essential features of the imposed piston movement were recovered, except for a limited backflow, which is also observed in cardiovascular applications.

The resulting Reynolds numbers, $Re = U_{max}D_0/\nu$ (U_{max} is the peak velocity at the orifice and ν is the kinematic viscosity) range from 5×10^3 to 1.5×10^4 depending on the specific program (similar values are obtained by using the limiting value of circulation, Γ, in Reynolds number computation, $Re_\Gamma = \Gamma/\nu$). The Strouhal numbers, $St = D_0/TU_{max}$, range from 0.06 to 0.19. These values are typical of applications to small aquatic animal pulsed jet locomotion and cardiac flows [27,28,16]. The specific values used for each velocity program, together with the stroke volume and effective stroke length, L_{max}/D_0, where L_{max} is the stroke volume divided by the orifice area, are listed in Table 1.

3. Results

3.1. Global flow behaviour

The four plots in Fig. 3 give an overview of the overall flow development for velocity program $s5$. This specific program was chosen since the behaviour looks qualitatively the same for all sets of PIV measurements. The figure shows the velocity and vorticity fields at four significant times during the piston cycle. On the whole, the snapshots describe the formation (first two plotted lines) and pinch-off (last plotted line) of the vortex ring. The evolution of the phenomenon suggests that the modulation of the flow rate at the orifice plays a fundamental role: for example, the vortex ring formation takes place when the acceleration is a maximum (at about 0.15 s; see also Fig. 2). In particular, it is worth noting that the vorticity layer connecting the orifice to the vortex ring becomes unstable as soon as the acceleration begins to diminish, during the last phase of the accelerated ejection (third plotted line). As a consequence it generates a series of small,

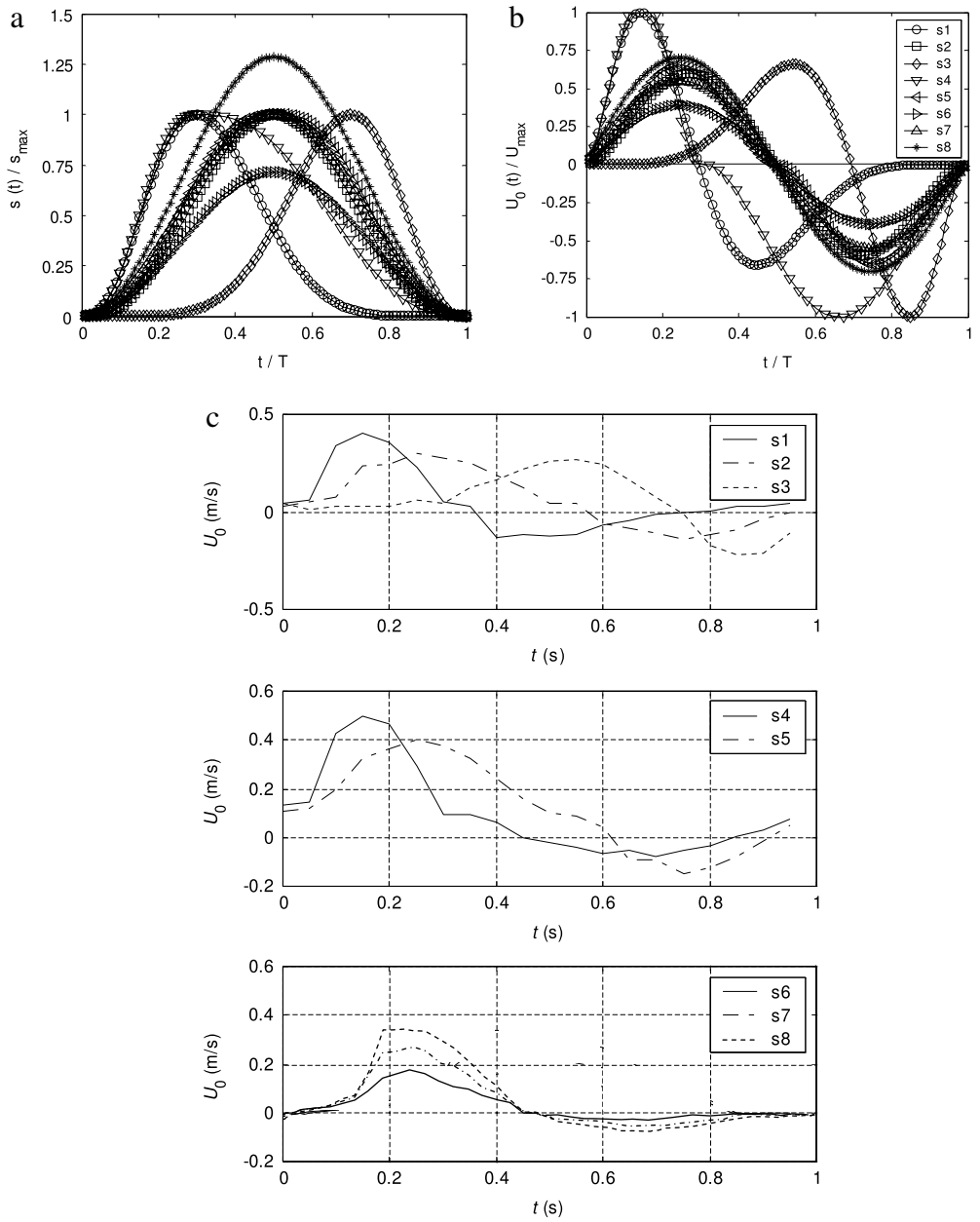

Fig. 2. Piston displacements (a) and velocities (b) for the tested programs ($s1, s2, \ldots, s8$). Measured mean exit velocities at the orifice (c). The relative error on velocity is 1%.

Table 1
Experimental conditions for the different tests.

Velocity program	Stroke volume (ml)	Effective stroke length L_{max}/D_0	Reynolds number	Strouhal number
s1	70	2.57	1.2×10^4	0.075
s2	70	3.25	8.9×10^3	0.10
s3	70	3.16	7.9×10^3	0.11
s4	70	3.73	1.5×10^4	0.060
s5	70	4.78	1.2×10^4	0.075
s6	50	2.16	4.8×10^3	0.19
s7	70	3.42	7.4×10^3	0.12
s8	90	4.58	1.0×10^4	0.088

aligned vortices (indeed vortex rings) during the next stages of the evolution. These structures do not seem to result from the gradual amplification of small perturbations, but they are formed just at the orifice edge. Nevertheless, this instability does not lead immediately to pinch-off; rather, the small vortices roll up and merge into the primary vortex ring (third plotted line). This is apparent also in the fourth plotted line, depicting the flow after the end of the accelerated ejection, immediately after the pinch-off: two vortices (**a** and **b**) are still moving along a spiral orbit around the primary vortex ring before they merge with it. Thus, the overall message from this global behaviour is that pinch-off takes place at about $t \approx 0.3$ s, i.e. once the maximum velocity

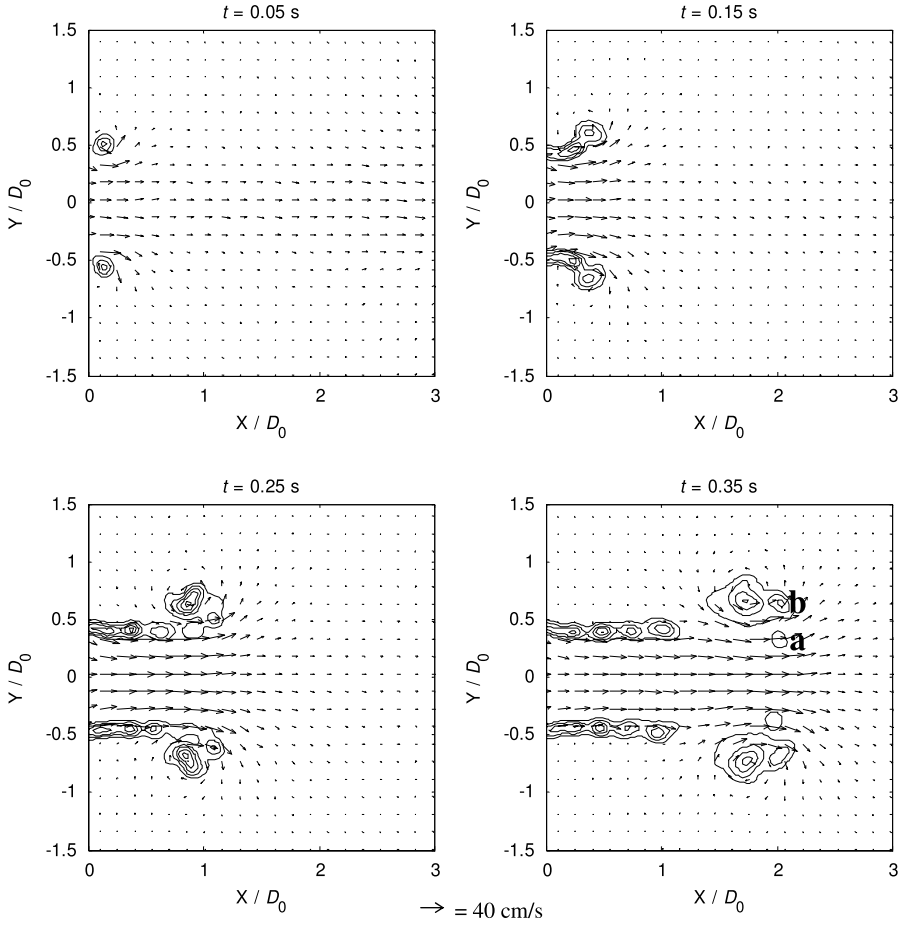

Fig. 3. Four snapshots of the velocity (arrows) and absolute value of the vorticity (contour lines) for the program s5. Contour lines of vorticity (made non-dimensional with the piston period, T) are plotted from 50 up to 300, with step 50. The letters **a** and **b** indicate two secondary vortices.

and vanishing acceleration are attained (compare to Fig. 2b,c for velocity program $s5$).

3.2. Slug model predictions

In order to have a simplified approach to compare with experimental data (especially in connection to the proposed scaling, presented in the next section) and a test to verify the relevance of viscous effects in the investigated phenomenon, the impulse conservation based "slug model" has been used [5,10,2,9,32]. This model has been already considered in other works on vortex rings, among others by Didden [33], Glezer [10] and Krueger [9]. However, in this case the model is applied over the entire evolution of the vortex ring from generation to free motion (i.e. during the piston accelerating phase, deceleration and rest). In the slug model, the flow is thought to be driven by a virtual piston of the same diameter as the orifice (sketched in the inset of Fig. 1). Therefore, the volume of the ejected fluid, at a given time, is computed as the product of the orifice area by the virtual piston displacement, $L(t)$ (Fig. 1), while $s(t)$ is used to indicate the specific piston program. The virtual displacement $L(t)$, and the circulation generated at the orifice, $\Gamma(t)$, are related to the velocity of the fluid at the orifice U_0 (which, in principle, equals the velocity of the piston except for the contraction ratio):

$$L(t) = \int_0^t U_0\left(t'\right) \mathrm{d}t' \tag{2}$$

$$\Gamma(t) = \frac{1}{2}\int_0^t U_0^2\left(t'\right) \mathrm{d}t'. \tag{3}$$

From dimensional arguments, the following relationships can be derived between the vortex circulation, Γ, vorticity, $\omega(t)$, and velocity, U_V [4]:

$$\Gamma(t) \approx U_V(t)\, D(t) \tag{4}$$

$$\omega(t) \approx U_V(t)\, \frac{D(t)}{\mathrm{d}^2(t)} \tag{5}$$

where $D(t)$ and $d(t)$ indicate the vortex ring and vortex core diameters, respectively. Moreover, the vortex position in time, $x_V(t)$, is given by

$$x_V(t) = \int_0^t U_V\left(t'\right) \mathrm{d}t' \approx \int_0^t \frac{\Gamma\left(t'\right)}{D\left(t'\right)} \mathrm{d}t'. \tag{6}$$

In previous equations, all quantities are assumed to change in time, except $D(t)$, which is considered as a constant equal to the orifice diameter D_0, as confirmed by experimental data.

From these equations, a prediction for the behaviour in time of a vortex ring is derived. The velocity, $U_0(t)$, measured experimentally is used in (2) and (3) to compute $L(t)$ and $\Gamma(t)$. Thus, by assuming $D(t) = D_0$, from (4) it is possible to derive $U_V(t)$, and from (6) the travel distance of the vortex, $x_V(t)$ (notice that multiplicative constants are not given for $U_V(t)$ and $x_V(t)$ and a factor, C_1, equal to 1 will be used). Lastly, Eq. (5) yields the vorticity, $\omega(t)$, once the behaviour of $d(t)$ is known (for example from experimental data).

Before drawing predictions, the proper non-dimensional time scales of the problem are discussed in detail in the next section.

3.3. Scaling

The formation process has been observed to scale with the orifice diameter, D_0, and the running mean of the exit velocity [33,10]:

$$u^*(t) = \frac{1}{t}\int_0^t U_0(t')\,dt' \tag{7a}$$

which is nothing less than $L(t)/t$. Choosing the orifice diameter, D_0, as length scale, a time scale can be defined:

$$t^*(t) = \frac{D_0}{u^*(t)} = \frac{D_0}{L(t)}t, \tag{7b}$$

which is non-trivially dependent on time t (through $L(t)$). Thus, the phenomenon can be described in terms of the non-dimensional time t/t^* (see, for example, [5]).

The previous scaling has been successfully applied to vortex motion before pinch-off [33,10,6,34]. Applying the scaling given in (7a) and (7b) after pinch-off as well, especially if the pinch-off time is not well determined, would yield a velocity scale that continues to change also when the vortex ring is completely formed and any further change in $U_0(t)$ is not relevant anymore.

As the velocity scale of the vortex ring is based on the exit velocity $U_0(t)$, one should only consider the time interval that contributes to the formation of the ring. Therefore, in computing the time scale, the integration of $U_0(t)$ should be stopped when the exit flow no longer influences the vortex ring. There are two main events that eventually stop this interaction: the first is the end of the ejection phase, the second is the achievement of a final evolution stage of the vortex ring, occurring at a critical value of the non-dimensional time t/t^*, which is known to depend on the shape of the program [6]. The occurrence of either event determines when the integration of (7a) and (7b) should stop. These criteria can be easily translated into practical rules in the case of schematic velocity programs, but they are not easy to apply for biological-like flows, since they vary gradually and are characterised by positive and negative accelerations that significantly affect the formation of vortex rings. As a consequence, in these kinds of flow, the limiting time is not simply related to general properties of the vortex rings, nor can it be related to the end of the ejection phase. In fact, the event marking the definitive disconnection between the vortex ring and the orifice jet, the pinch-off, has been observed to occur between the time at which the maximum ejection velocity is attained ($dU_0/dt = 0$) and the end of the ejection ($U_0 = 0$) (as in the discussion of Fig. 3).

Analysis of the present experimental data suggests that, for gradually varied flows, accelerated ejection is mostly relevant to the formation of the vortex ring. Following this idea, we proposed interrupting the integration of (7a) at a time, t_a, slightly after the positive acceleration phase ends. In practice, this corresponds to the time when the quantity $L(t)/t = u^*(t)$ is maximum, i.e. when

$$\frac{d}{dt}\left(\frac{1}{t}\int_0^t U_0(t')\,dt'\right) = 0,$$

or, correspondingly, when

$$U_0(t_a) = \frac{L(t_a)}{t_a} = u^*(t_a). \tag{8}$$

The meaning of Eq. (8) is the following. While the average velocity of the ejected fluid column, u^*, is smaller than the instantaneous ejection velocity, U_0, the vortex is still connected to the orifice by a vorticity layer. Conversely, when $u^*(t) > U_0(t)$, the fluid ejected from the orifice at velocity $U_0(t)$ is no longer able to feed the previously ejected fluid moving at velocity $u^*(t)$. Thus, the time when the two previous velocities are equal identifies the end of the influence of the orifice flow on the vortex ring and vortex pinch-off. The time $t = t_a$ is univocally and easily determined by the specific velocity program. The use of non-dimensional time and velocity scales based on this consideration allows the description of the entire vortex dynamics (generation, pinch-off and subsequent evolution). Therefore, in relation to (7a) and (7b), we can choose the velocity and time scales as follows:

$$u_*(t) = \begin{cases} \dfrac{1}{t}\displaystyle\int_0^t U_0(t')\,dt' = u^*(t) & \text{for } t \le t_a \\ \dfrac{1}{t_a}\displaystyle\int_0^{t_a} U_0(t')\,dt' = u^*(t_a) & \text{for } t > t_a, \end{cases} \tag{9a}$$

$$t_*(t) = \begin{cases} \dfrac{D_0}{u^*(t)} = \dfrac{D_0}{L(t)}t & \text{for } t \le t_a \\ \dfrac{D_0}{u^*(t_a)} = \dfrac{D_0}{L(t_a)}t_a & \text{for } t > t_a, \end{cases} \tag{9b}$$

where the time t_a is defined by Eq. (8).

It is worth noting that, in principle, the previous scaling is not different from the one proposed by Didden [33], Glezer [10], and Gharib et al. [6] and generalised by Dabiri and Gharib [34] to account for time-varying velocity. However, the main question is to find a reliable method for choosing the time when the influence of the flow from the orifice ends and the integration of Eqs. (7a) and (7b) should be interrupted. The proposed criterion, given by Eq. (8), makes it possible to identify this precise instant in a simple way for any velocity program and to unequivocally describe the entire process of vortex generation, detachment and free motion.

The vortex position, circulation and peak vorticity can be non-dimensionalised by using the previous velocity and time scales (7a) and (7b) or (9a) and (9b). While the dimensional time t increases continuously, the non-dimensional time t/t^* could also decrease (due to the reduction of $L(t)$ during backflow) and the non-dimensional time t/t_* always increases monotonically (since t_* is a constant for $t > t_a$). This must be considered when examining the results presented in the next sections.

From the slug model presented in the previous section, it is possible to derive a simple prediction of the behaviour of non-dimensional quantities by assuming an increasing power law for $U_0(t)$ (using (7a) and (7b)) and by approximating $D(t)$ with D_0:

$$\begin{aligned} &\frac{x_V(t)}{D_0} \approx \left(\frac{t}{t^*}\right)^2 \\ &\frac{\Gamma(t)}{u^*(t)\,D_0} \approx \frac{U_V(t)}{u^*(t)} \approx \left(\frac{t}{t^*}\right) \\ &\omega(t)\,t^*(t) \approx \left(\frac{t}{t^*}\right)\frac{1}{d^2(t)}, \end{aligned} \tag{10a}$$

where the multiplicative coefficients are dependent on the specific power law used. Thus, initially the position of the vortex increases as the square of the non-dimensional time, while the non-dimensional circulation increases in a linear manner and the non-dimensional peak vorticity as $(t/t^*)^{-1}$, if $d(t)$ is dependent in a linear manner on t/t^* (as reported in the following).

On the other hand, for a decreasing power law for $U_0(t)$ (using (9a) and (9b)) and by determining the time t_a by means of (8), the following predictions are obtained:

$$\begin{aligned} &\frac{x_V(t)}{D_0} \approx \left(\frac{t}{t_*}\right) \\ &\frac{\Gamma(t)}{u_*(t)\,D_0} \approx \text{const} \\ &\omega(t)\,t_*(t) \approx \frac{1}{d^2(t)}; \end{aligned} \tag{10b}$$

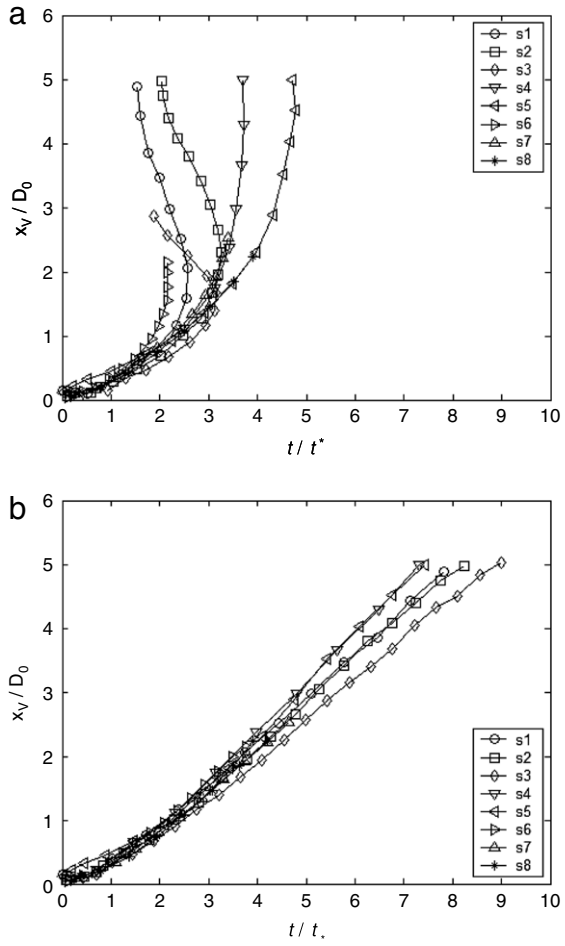

Fig. 4. Non-dimensional vortex position as a function of time for the eight tested programs. Time t is made non-dimensional by t^* in (a) and by t_* in (b). The relative error on position is 2%.

i.e. the vortex position increases linearly with the non-dimensional time t/t_*, whereas the circulation is almost constant. With $d(t)$ depending linearly on t/t_* (as reported in the following), the non-dimensional vorticity decreases with $(t/t_*)^{-2}$. For velocity programs, $U_0(t)$, that are more complicated than a simple increasing or decreasing power law, predictions are still possible (even if not always in analytic form). These predictions are plotted together with experimental results in the next sections. In these cases, differences between time scales using (7b) or (9b) are pointed out and compared to the relations (10a) and (10b).

3.4. Vortex ring position and motion

The proposed scaling is verified through the analysis of the experimental data describing the vortex ring motion. These data are also compared with predictions based on the "slug model" (described in Sections 3.2 and 3.3). The vortex core position was found from the positive and negative maxima of the vorticity on the measuring plane; the downstream travel distance was computed as the average of the two positions. In Fig. 4, the position of the vortex ring was plotted as a function of time for the eight tested piston programs: in Fig. 4a, the time is made non-dimensional by means of the time scale t^* (after integration of Eqs. (7a) and (7b) over the whole time history), whereas the time scale t_*, as defined in (9b), was used in Fig. 4b.

In Fig. 4a, the different curves diverge and behave in a non-linear manner as t/t^* exceeds about 1.5 already during the accelerating phase. This corroborates the prediction of Eq. (10a) in which a quadratic behaviour is expected (as above mentioned, t/t^* also decreases after this time). The observed divergence between the results from different velocity programs also suggests that the end of the influence of the orifice flow on the vortex ring formation depends mainly on the shape of the velocity program. Conversely, using the scaling proposed in Eq. (9b), Fig. 4b, all data collapse on a line for the complete series of velocity programs (a deviation around 10% is still present for $t/t_* > 5$, presumably based on the uncertainty in the experimental evaluation of t_a), suggesting that time t_* is the proper scale for the whole phenomenon of vortex ring generation, pinch-off and successive development. For $t > t_a$, the behaviour is nearly linear, as predicted by (10b).

It is interesting to compare the experimental results with the specific predictions of the "slug model" (and not only in terms of general trends as in Eqs. (10a) and (10b)). In Fig. 5a, the non-dimensional vortex positions for different programs are plotted as a function of the non-dimensional time t/t^* together with predictions obtained from relation (6) using (3), and assuming a constant of proportionality equal to 1 (for the sake of clarity only four programs out of eight are presented). The agreement between the model and the data is quite good for all programs (especially for $s1$ and $s6$) in both the accelerating phase and the decelerating phase. In performing this comparison, it must be considered that the slug model is a pure inviscid "ideal" model which should not reproduce the experimental data exactly. Moreover, the predictions of the slug model confirm that the time scale t^* is a correct scaling parameter before pinch-off (the predictions and experimental data are very close one to each other), while it is not particularly suited for the subsequent phases. In Fig. 5b, vortex positions are plotted as functions of non-dimensional time t/t_*. In this case, the data corresponding to different programs collapses quite well, and almost linear behaviour is observed after the accelerating phase. This confirms that the time t_* allows for the proper scaling of the data and that the model predictions accurately reproduce the behaviour of experimental data, even if the slopes are different. This difference in slope depends on the fact that the no multiplicative constant, C_1, is present in relation (6), so that it is assumed that $C_1 = 1$. To account for the differences between the present data and model predictions reported in Fig. 5b, it seems that in (6) $C_1 \sim 2.2$, almost independently of the specific program. We stress again that the time when the exit flow no longer influences the vortex ring (which is the point where the curves end the quadratic growth and continues as a straight line) is just $t = t_a$ (determined from (8)).

From the above data on vortex positions, the vortex travel velocity, U_v, has been computed by central differences. It should be expected that the non-linear quadratic phase should give a linear increase of the velocity and that the linear increase of the position after "pinch-off" should result in a constant travel velocity. In Fig. 6, the vortex travel velocity made non-dimensional by the velocity scale $u_*(t)$ (Eq. (9a)) is presented for the different velocity programs. The results follow quite closely with what was expected from previous data on vortex position in time (as the position is increasing linearly for $3 < t/t_* < 7$, accordingly the travel velocity is about constant) with differences within 20%. For $t/t_* > 5$, the velocity tends to decrease, which is consistent with the free motion of the vortex ring after pinch-off taking into account viscous effects [2]. As for the vortex position in time, even for the velocity, the proposed scaling allows a collapse of data of the different velocity programs on a single curve describing a universal evolution of the phenomenon. Notice that Eq. (4) indicates that the behaviour of the vortex velocity is exactly the same as that of vortex circulation, except for the (nearly constant) quantity $D(t) = D_0$ and for a multiplicative constant. Thus, in the next section, slug model predictions will be compared with measurements of vortex circulation (which does not depend on arbitrary multiplicative constants in relation (3)).

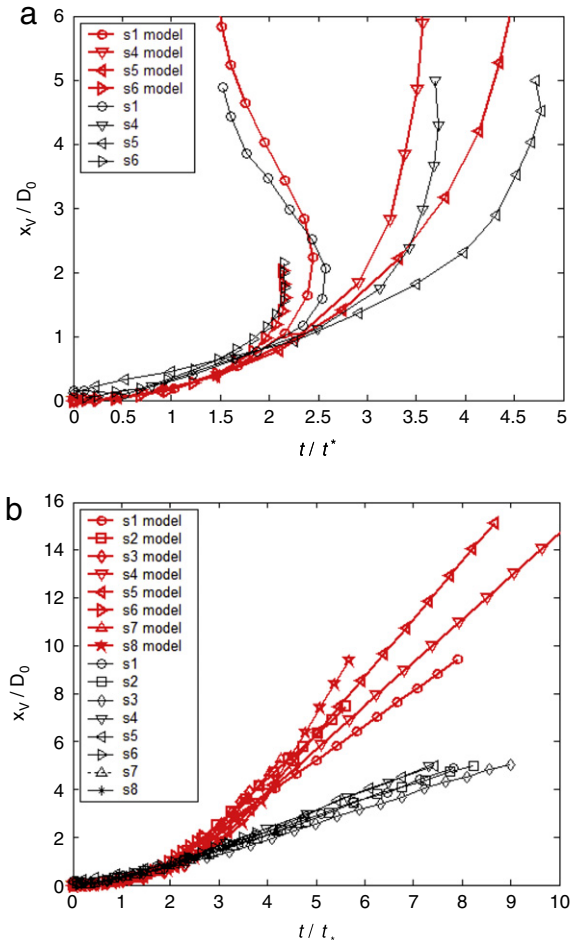

Fig. 5. Non-dimensional vortex position as a function of time for some of the tested programs. Time t is made non-dimensional by t^* in (a) and by t_* in (b). Comparisons between model predictions (red lines) and experimental data (black lines). The relative error on position is 1%. (For interpretation of the references to colour in this figure legend, the reader is referred to the web version of this article.)

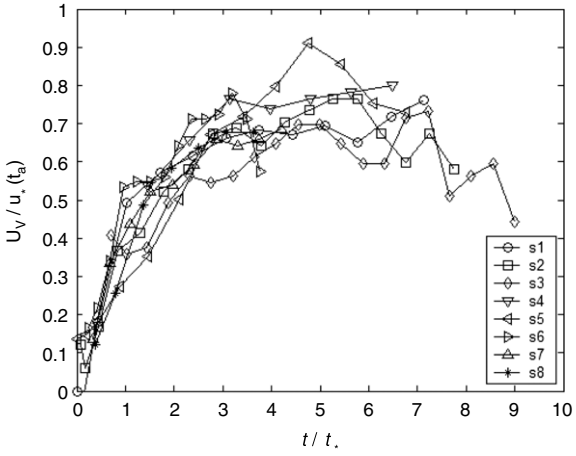

Fig. 6. Non-dimensional vortex travel velocity as a function of non-dimensional time t_* for the eight piston programs. The relative error on vortex velocity is 4%.

3.5. Vortex circulation, radius and vorticity

In order to compute the properties of the resulting vortex ring, its cross-sectional area on the measurement plane has to be identified. To this end, the discriminant, Δ, of the 2D strain-rate tensor has been computed over the measurement plane [35].

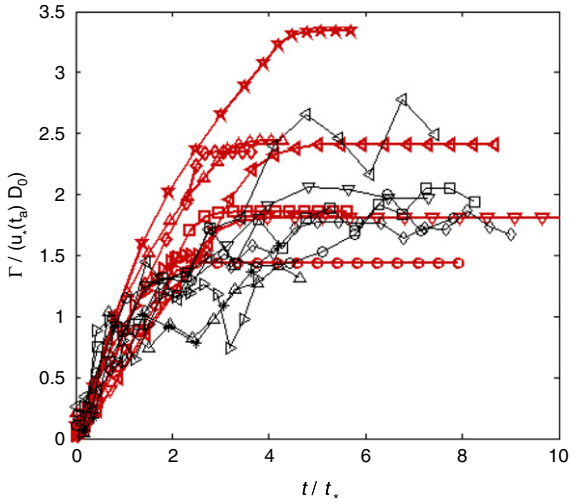

Fig. 7. Non-dimensional vortex circulation as a function of non-dimensional time for the eight piston programs. Comparisons between model predictions (red lines) and experimental data (black lines). Symbols as in Fig. 5. The relative error on circulation is 3%. (For interpretation of the references to colour in this figure legend, the reader is referred to the web version of this article.)

Negative values of Δ indicate the presence of a vortex. Then, the cross-sections are taken as the areas, around the maximum and minimum of the vorticity, where $\Delta < 0.1\Delta_{min}$, with Δ_{min} indicating the minimum of the discriminant on the measured field.

Once the vortex has been identified, its main features can be derived. Fig. 7 shows the non-dimensional vortex circulation, Γ_v, as a function of the non-dimensional time. The circulation, Γ_v, was obtained by integrating the vorticity over the vortex area, and made dimensionless using the scale $u_*(t)D_0$. In every tested case, the circulation, after an initial increase, reached a plateaux ranging from 1.5 to 3, depending on the specific velocity program. The initial increase ended at t/t_* roughly equal to 4, i.e. when the vortex ring reached its maximum velocity (as above stated the two quantities are closely related). This behaviour is in agreement with the model prediction of Eq. (10a) during accelerated ejection (in this phase the time scale t_* is equivalent to t^*). After that instant, which roughly corresponds to the "pinch-off", the circulation remained nearly constant, in agreement with the Kelvin theorem (at this time the proposed time and velocity scales are simply constant), with predictions from (10b) and with findings from other authors (obtained also for impulsive or rapidly changing forcing) [7,6]. The measured and predicted time for reaching the limiting constant value of the circulation is t/t_* between 3 and 4 which closely agrees with the so-called "formation time" proposed by Gharib et al. [6].

The limiting constant values predicted by the slug model are in close agreement with experimental data. This means that the limiting value of circulation of the vortex ring generated by a given velocity program can be predicted using a very simple model. This fact has important consequences for the modelling of flow fields which can be assimilated to pulsed jets through orifices.

The peak vorticity is related to circulation by Eqs. (4) and (5) and measurements can be compared with model predictions, once the vortex core diameter, $d(t)$, is known. In Fig. 8, the latter is plotted (non-dimensionalised by the orifice diameter) for the eight piston programs. After a short transitional phase, the diameter increases in a linear manner as t/t_* for all velocity programs.

The values of $d(t)$ were used in Eq. (5) to provide a prediction of the non-dimensional peak vorticity shown together with experimental data in Fig. 9 (as in the previous Figs. 7 and 8, the vorticity and time are made non-dimensional by using scales computed slightly after the end of the accelerated ejection). The peak vorticity

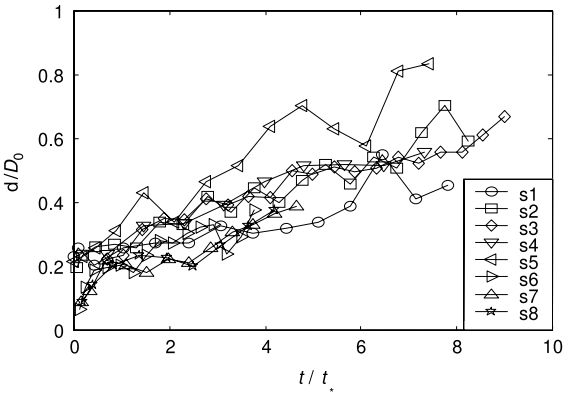

Fig. 8. Non-dimensional vortex diameter as a function of time for the eight piston programs. The relative error on diameter is 2%.

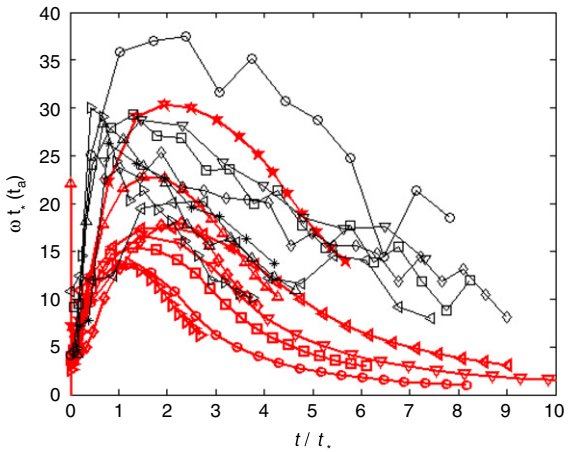

Fig. 9. Non-dimensional peak vorticity as a function of non-dimensional time for the eight tested piston programs. Comparisons between model predictions (red lines) and experimental data (black lines). Symbols as in Fig. 5. The relative error on vorticity is 7%. (For interpretation of the references to colour in this figure legend, the reader is referred to the web version of this article.)

is measured by taking the maximum vorticity value in the vortex cross-sectional area. As mentioned in Section 3.3, from Eq. (10a) it is possible to state that the peak vorticity should decrease as the inverse of the non-dimensional time for $t \leq t_a$ and as $(t/t_*)^{-2}$ for larger non-dimensional times. The results plotted in Fig. 9, confirm this prediction: the peak vorticity, ω, at the centre of the vortices tends to decrease after the steep initial growth. The collapse of the data on a common behaviour is not as good as for the vortex position (Figs. 4 and 5) and circulation (Fig. 7). In this case, the vertical dispersion of the data is mainly due to the differentiation of experimental data. Nevertheless, the different velocity programs give similar temporal trends, confirming that the time t_* scales the phenomenon properly. The slug model also rather successfully predicts the experimental values of peak vorticity during the deceleration of ejection velocity (thus indicating that the multiplicative constant in relation (5) is nearly equal to 1).

4. Discussion and conclusions

A criterion for evaluating the time scaling of vortex rings in the case of gradually varying flows has been proposed. It is based on the experimental observation of eight different velocity programs, generating vortex rings through a thin-edged orifice. The velocity programs were selected in relation to applications concerning cardiac flows and pulsed locomotion of aquatic animals.

Indeed, the case of gradual variation of orifice flows is at the same time representative of a wide range of biological flows, such as intraventricular flows, jet propulsion of squids and jellyfishes, amongst others, and is challenging since the flow modulation results in accelerations and decelerations of the exit flow that influence the formation process.

On the basis of the present experiments, a criterion has been proposed in order to compute the time when the vortex ring is no longer influenced by the orifice flow. This has been observed to happen when the average velocity of the fluid column ejected from the orifice exceeds the instantaneous velocity at the orifice. This condition is reached when the average ejection velocity attains a maximum. That time is determined univocally from the given velocity program and is observed to take place slightly after the end of the accelerated ejection.

In other words, while the instant of pinch-off does not have a unique definition (because it is dependent on the iso-vorticity line considered) and it is difficult to determine experimentally (since time and space resolved velocity measurements are required in addition to the high sensitivity to measurement noise), the proposed criterion is easily and univocally determined from the velocity program itself. The proposed criterion accounts not only for scaling during vortex formation, but also during pinch-off and further vortex motion.

The analysis of motion, and of other important characteristics of vortex rings, confirms that time, t_*, is a proper scale for the phenomenon also in the quite complicated case of the gradual variation of piston velocity. At the same time, it is useful to easily estimate the instant when the influence of the orifice flow on the vortex ring comes to an end. This result is applicable to any physical system which generates vortices recursively.

The experimental results and the proposed scaling were discussed also with the help of the so-called "slug model", which only implies the knowledge of the velocity program under the assumption of total impulse conservation, making it possible to derive predictions for the vortex position, circulation and peak vorticity in time. These predictions (which also have analytical forms in the case of velocity programs expressed in terms of simple power laws) are in close agreement with experimental data, thus suggesting that the total impulse is more or less conserved and viscous effects are negligible even during accelerated ejection phases.

Acknowledgements

The authors are grateful to Dr. Francisco Pereira for helpful comments and suggestions. This work was partially funded by the Ministero Università e Ricerca, PRIN 2006-prot. 2006087719.

References

[1] T.T. Lim, T.B. Nickels, Vortex rings, in: S.I. Green (Ed.), Fluid Vortices, Kluwer Academic Publisher, 1995, pp. 87–147.
[2] K. Shariff, A. Leonard, Vortex rings, Ann. Rev. Fluid Mech. 24 (1992) 235–279.
[3] C. Tung, L. Ting, Motion and decay of a vortex ring, Phys. Fluids 10 (5) (1967) 901–910.
[4] P.G. Saffman, The velocity of viscous vortex rings, Stud. Appl. Math. 49 (1970) 371.
[5] D.I. Pullin, Vortex ring formation at tube and orifice openings, Phys. Fluids 22 (3) (1979) 401–403.
[6] M. Gharib, E. Rambod, K. Shariff, A universal time scale for vortex ring formation, J. Fluid Mech. 360 (1998) 121–140.
[7] K. Mohseni, M. Gharib, A model for universal time scale of vortex ring formation, Phys. Fluids 10 (10) (1998) 2436–2438.
[8] F.B. Kaplanski, Y.A. Rudi, A model for the formation of optimal vortex rings taking into account viscosity, Phys. Fluids 17 (87101) (2005) 1–7.
[9] P.S. Krueger, An over-pressure correction to the slug model for vortex ring circulation, J. Fluid Mech. 545 (2005) 427–443.
[10] A. Glezer, The formation of vortex rings, Phys. Fluids 31 (12) (1988) 3532–3542.
[11] M. Kumar, J.H. Arakeri, P.N. Shankar, Translational velocity oscillations of piston generated vortex rings, Phys. Fluids 7 (11) (1995) 2751–2756.

[12] J. Borée, N. Atassi, G. Charnay, L. Taubert, Measurements and image analysis of the turbulent field in an axisymmetric jet subject to a sudden velocity decrease, Exp. Therm. Fluid Sci. 14 (1997) 45.
[13] A. Weigand, M. Gharib, On the decay of a turbulent vortex ring, Phys. Fluids 6 (12) (1994) 3806–3809.
[14] D. Fabris, D. Liepmann, Vortex ring structure at late stages of formation, Phys. Fluids. 9 (9) (1997) 2801–2803.
[15] A. Dazin, P. Dupont, M. Stanislas, Experimental characterization of the instability of the vortex ring. Part I: linear phase, Exp. Fluids 40 (2006) 383–399.
[16] P.S. Krueger, M. Gharib, The significance of vortex ring formation to the impulse and thrust of a starting jet, Phys. Fluids 15 (5) (2003) 1271–1281.
[17] M. Rosenfeld, E. Rambod, M. Gharib, Circulation and formation number of laminar vortex rings, J. Fluid Mech. 376 (1998) 297–318.
[18] M. Shusser, M. Rosenfeld, J.O. Dabiri, M. Gharib, Effect of time-dependent piston velocity program on vortex ring formation in a piston/cylinder arrangement, Phys. Fluids 18 (2006) 1–6.
[19] R.E. Breidenthal, The turbulent exponential jet, Phys. Fluids 29 (1986) 2346.
[20] Q. Zhang, H. Johari, Effect of acceleration on turbulent jets, Phys. Fluids 8 (1996) 2185.
[21] S.C. Shadden, J.O. Dabiri, J.E. Marsden, Lagrangian analysis of fluid transport in empirical vortex ring flows, Phys. Fluids 18 (047105) (2006) 1–11.
[22] E.J. Anderson, M.A. Grosenbaugh, Jet flow in steadily swimming adult squid, J. Exp. Biol. 208 (2005) 1125–1146.
[23] H. Bot, J. Verburg, B.J. Delemare, J. Strackee, Determinants of the occurrence of vortex rings in the left ventricle during diastole, J. Biomech. 23 (1990) 607–615.
[24] J. Cooke, J. Hertzberg, M. Boardman, R. Shandas, Characterizing vortex ring behaviour during ventricular filling with Doppler echocardiography: an in vitro study, Ann. Biomed. Eng. 32 (2) (2004) 245–256.
[25] I. Danaila, J. Helie, Numerical simulation of the postformation evolution of a laminar vortex ring, Phys. Fluids 20 (073602) (2008).
[26] T. Maxworthy, Some experimental studies of vortex rings, J. Fluid Mech. 81 (1977) 465–495.
[27] Ch. Brucker, U. Steinseifer, W. Schroder, H. Reul, Unsteady flow through a new mechanical heart valve prosthesis analysed by digital particle image velocimetry, Meas. Sci. Technol. 13 (2002) 1043–1049.
[28] G. Bolzon, L. Zovatto, G. Pedrizzetti, Birth of three-dimensionality in a pulsed jet through a circular orifice, J. Fluid Mech. 493 (2003) 209–218.
[29] C.A. Taylor, M.T. Draney, Experimental and computational methods in cardiovascular fluid mechanics, Annu. Rev. Fluid Mech. 36 (2004) 197–231.
[30] M.D. De Tullio, A. Cristallo, E. Balaras, R. Verzicco, Direct numerical simulation of the pulsatile flow through an aortic bileaflet mechanical heart valve, J. Fluid Mech. 622 (2009) 259–290.
[31] P.F. Linden, J.S. Turner, 'Optimal' vortex rings and aquatic propulsion mechanisms, Proc. Roy. Soc. London B. 271 (2004) 647–653.
[32] R.N. Abani, N.D. Reitz, Unsteady turbulent round jet and vortex motion, Phys. Fluids 19 (125102) (2007).
[33] N. Didden, On the formation of vortex ring: rolling-up and production of circulation, J. Appl. Math. Phys. 30 (1979) 101–116.
[34] J.O. Dabiri, M. Gharib, The formation number of vortex rings formed in uniform background co-flow, J. Fluid Mech. 556 (2006) 147–166.
[35] A..E. Perry, M.S. Chong, Topology of flow patterns in vortex motions and turbulence, Appl. Sci. Res. 53 (3–4) (1994) 357–374.